frontiers | Frontiers in Chemical Biology

TYPE Original Research
PUBLISHED 22 July 2024
DOI 10.3389/fchbi.2024.1408621

OPEN ACCESS

EDITED BY
Michal Jan Gajda,
Migamake Pte Ltd., Singapore

REVIEWED BY
Kittikhun Wangkanont,
Chulalongkorn University, Thailand
Nipanshu Agarwal,
National Institute of Diabetes and Digestive and Kidney Diseases (NIH), United States
Kevin Leung,
University of California, San Francisco, United States

*CORRESPONDENCE
Dubravka Drabek,
d.drabek@erasmusmc.nl

RECEIVED 02 April 2024
ACCEPTED 17 June 2024
PUBLISHED 22 July 2024

CITATION
Janssens R, van Haperen R, van der Reijden M, Maas A, Wang J, Grosveld F and Drabek D (2024), Generation and preclinical evaluation of a human heavy-chain-only antibody recognizing the membrane-bound tumor-associated antigen mesothelin.
Front. Chem. Biol 3:1408621.
doi: 10.3389/fchbi.2024.1408621

Generation and preclinical evaluation of a human heavy-chain-only antibody recognizing the membrane-bound tumor-associated antigen mesothelin

Rick Janssens[1,2], Rien van Haperen[1,2], Michael van der Reijden[1,2], Alex Maas[1], Jingsong Wang[3], Frank Grosveld[1,2] and Dubravka Drabek[1,2]*

[1]Department of Cell Biology, Erasmus MC, Rotterdam, Netherlands, [2]Harbour BioMed, Rotterdam, Netherlands, [3]Harbour BioMed, Shanghai, China

Objective: Mesothelin (MSLN) is an attractive target for anticancer therapeutics and bioimaging reagents that utilize antibodies. This study was aimed at developing a novel human anti-MSLN single-domain antibody that exclusively binds to the membrane-attached MSLN using transgenic mice generating human heavy-chain-only antibodies (HCAbs) and exploring the resulting HCAbs as imaging tools.

Methods: We introduced a doxycycline-inducible human MSLN gene in genetically modified mice expressing human HCAbs. This new method of non-invasive immunization by antigen induction results in MSLN antigen production in its native conformation on the cell surface. Screening of 2,000 HCAbs from the resulting immune library yielded numerous binders, from which we chose 19G6 as the lead antibody. This antibody was ^{111}Indium radiolabeled and tested in a xenotransplantation tumor model with OVCAR-3 cells.

Results: The 19G6 antibody shows nanomolar affinity toward membrane-bound MSLN and does not recognize soluble MSLN. The human MSLN-positive tumors were visualized in an *in vivo* mouse model. The non-labeled antibody prevented binding when provided in excess, showing tumor specificity.

Conclusion: 19G6 with a human Fc is a promising tumor-cell tracer *in vivo*. This HCAb can also be engineered into a smaller and shorter-lived tracer (only the VH domain) or combined with other target-binding domains to form multispecific modalities for tumor immunotherapy.

KEYWORDS

mesothelin (MSLN), heavy-chain-only antibody (HCAb), OVCAR-3 tumor, radioimaging, SPECT and PET imaging

1 Introduction

Fully human antibodies in different shapes and formats, such as the classical monoclonal heavy- and light-chain tetrameric antibodies (MoAbs), heavy-chain-only antibodies (HCAbs), single-chain antibodies (scFvs), single-domain antibodies (sdAbs), multispecific antibodies, but also antibody mimetics, and affibodies, have emerged as next-generation therapeutics and diagnostics, especially in oncology (Liu and Chen, 2022). In the ideal situation, antibodies should be tumor-selective to avoid binding to healthy tissues. Mesothelin (MSLN) was discovered during the identification of novel cell-surface markers for ovarian cancer, and the first antibody binding to MSLN was the mouse antibody K1 (Chang et al., 1992). MSLN is a membrane-bound anchored glycoprotein that is normally expressed at low levels on mesothelial cells of the pleura, pericardium, and peritoneum. However, it is a tumor-associated antigen (TAA) because it is highly overexpressed in mesotheliomas (lung tumors of mesothelial origin), ovarian and pancreatic carcinomas, and to a lesser degree in several other human cancers (Hassan and Ho, 2008; Pastan and Hassan, 2014; Hassan et al., 2016). An upstream enhancer was identified that strongly activates an otherwise weak promoter by binding to the transcription factor TEF1 in tumors, causing MSLN overexpression in pancreatic and other cancers (Hucl et al., 2007). The biological role of MSLN is still largely unknown. The gene encodes for a 71-kDa precursor protein, which is further processed to the N-terminal ~31-kDa megakaryocyte potentiating factor (MPF) and ~40-kDa C-terminal membrane-bound mature MSLN (Zhang et al., 2014). Interactions with Mucin-16 that is also frequently co-overexpressed in ovarian cancer, malignant mesothelioma, and pancreatic cancer are reported to be involved in some aspects of cancer progression and metastasis (Gubbels et al., 2006; Hassan et al., 2010; Chen et al., 2013; Rottey et al., 2022). Antibodies blocking these interactions have been reported to be of therapeutic value (Kaneko et al., 2009; Ho et al., 2011). The CA125 epitope of Mucin-16 that is involved in the interaction with MSLN is commonly used as a prognostic marker in the follow-up of patients treated for ovarian cancers (Dochez et al., 2019), while MSLN is used as a diagnostic and prognostic marker in ovarian cancer and lung mesothelioma (Scholler et al., 1999; Robinson et al., 2003; Hassan et al., 2006; Hollevoet et al., 2012). Elevated serum levels of these markers are caused by shedding of soluble MSLN (sMSLN) from the cancer cells. While sMSLN measurement is a reliable prognostic test for cancer progression, the shedding of sMSLN causes problems for both therapy and imaging when an anti-MSLN antibody binds to not only tumor cells but also circulating sMSLN that acts as a decoy. Several approaches have been investigated in animal models and clinical trials for targeting MSLN, like antibody-dependent cellular cytotoxicity, conjugates with immunotoxin and drugs, and chimeric antigen receptor T (CAR-T) cells (Rottey et al., 2022; Faust et al., 2022; Grasso et al., 2023; Sun et al., 2023). Most of the antibodies described in literature do not bind to the C-terminal membrane-bound region III/IV of MSLN but to similar or overlapping epitopes on the N-terminal portion of MSLN, such as amatuximab and anetumab, which are the two most investigated anti-MSLN antibodies in clinical trials. It was believed that epitopes close to the cell surfaces may be occluded and difficult to access by full-sized immunoglobulins. A plethora of different antibody libraries has been developed, including scFv from immunized wild-type mice and genetically modified mice expressing human variable domains or from immune llama libraries, synthetic human single-domain (VH) libraries using specific immunizations, and tolerance induction schemes and library screening protocols, with the aim of obtaining antibodies that can selectively bind to membrane-bound MSLN. A limited number of studies have resulted in such antibodies (Tang et al., 2013; Zhang et al., 2015; Asgarov et al., 2017; Lin et al., 2023). Reduced shedding of the surface MSLN was shown to improve the efficacy of MSLN targeting with immunotoxins (Awuah et al., 2016). Recently, an antibody (15B6) was described, which prevents shedding by binding to the major protease cleavage sites at the C terminus of MSLN, and was fabricated as an active chimeric receptor whose activity was not blocked by the shed MSLN in the mouse model (Zhan et al., 2023; Liu et al., 2024). Finally, full characterization of the epitopes bound by many of the antibodies is lagging in antibody discovery because data on the structure of full MSLN and its conformational variability are still lacking (Zhan et al., 2023).

Herein, we report a new immunization strategy to obtain "difficult to find" antibodies, which in our case is an antibody that specifically binds membrane-bound MSLN. We show that oral doxycycline-induced expression of human MSLN results in immunization of Harbour HCAb transgenic mice (harbourbiomed.com/technology) and isolation of fully human anti-MSLN HCAbs. We selected and characterized 19G6 as the most promising HCAb that exclusively binds membrane-attached human MSLN. We tested ^{111}Indium-radiolabeled 19G6 in an *in vivo* OVCAR-3 xenotransplantation model in nude mice to show its specific targeting ability for tumor imaging and potential use for therapy.

2 Materials and methods

2.1 Generation of MSLN-inducible transgenic mouse lines producing human HCAbs

The total RNA was obtained from NIH OVCAR-3 cells using TRIzol reagent (Sigma-Aldrich, St. Louis, MO, United States) according to the manufacturer's instructions, and cDNA was prepared using the oligo (dT) $_{12-18}$ primer using Superscript ^{TM}II (Invitrogen) according to the manufacturer's protocols. The human MSLN precursor cDNA sequence (including secretion signal, MPF, furin cleavage site, and MSLN with GPI anchor) was amplified from cDNA using the following PCR primers: MSLN s: 5′-GCTAGATCTGCCGCCACCATGGCCTTGCCAACGGCT and MSLN as: 5′- CTCAAGCTTTCAGGCCAGGGTGGAGGCTAG. The amplified fragment was digested with Bgl II/Hind III restriction enzymes (underlined) and cloned onto BamHI (having compatible cohesive ends with BglII)/Hind III cut pTRE vector (Clontech). The resulting plasmid was sequenced, and the correct sequence was confirmed (Q13421 MSLN_HUMAN). The plasmid was linearized by Sca I digest, gel-purified, and injected at a concentration of 2 ng/μL in a buffer (5 mM TRIS/0.1 mM EDTA, pH=7.4) into fertilized oocytes of HCAb 2.1 Harbour transgenic mice (Nonabio.com/

10.3389/fchbi.2024.1408621

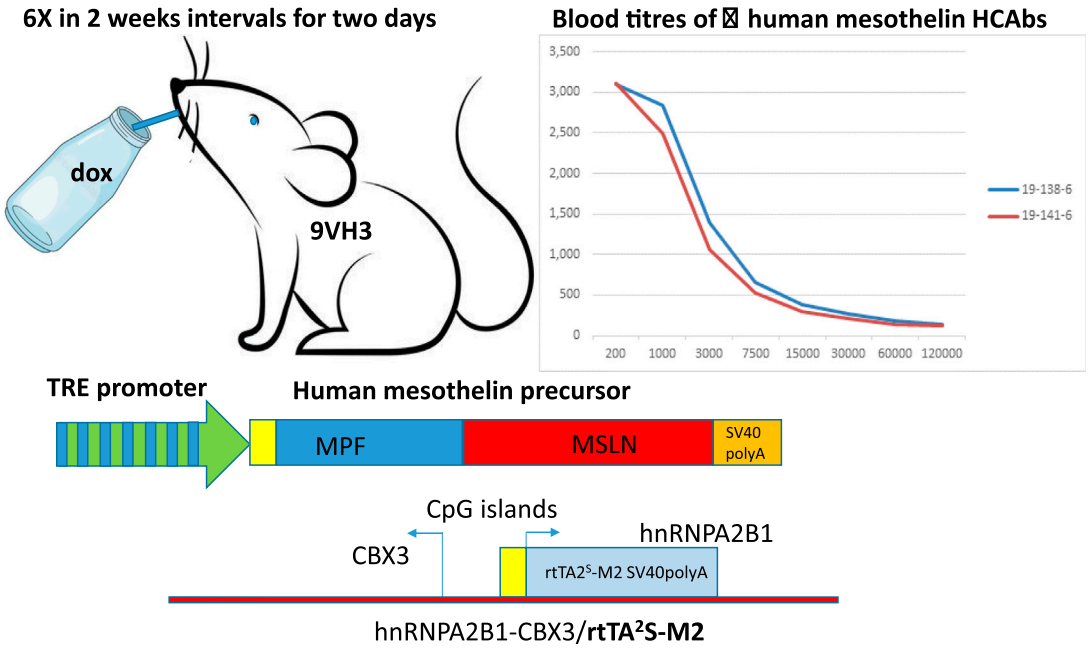

FIGURE 1
Schematic representation of doxycycline-inducible immunization. HBM 9VH3 mice are double positive for two transgenes, i.e., components necessary for the Tet-On system: one containing a tetracycline responsive element (TRE) (seven repeats of TetO separated by spacer) placed upstream of a minimal promoter driving expression of human mesothelin and the other ubiquitously expressing the rtTA2^{S}-M2 transactivator. The rtTA protein is capable of binding the operator only if bound by tetracycline-analog doxycycline (dox). The introduction of doxycycline to the system initiates transcription and expression of human mesothelin. There is no leakiness and no expression of the human mesothelin unless doxycycline is provided (via drinking water every 2 weeks for 2-day periods). This regimen is repeated six times. Pulsed expression of human mesothelin causes immune reactions leading to antibody production, as seen in two different mice through human-mesothelin-specific ELISA.

technology) containing ubiquitously expressed rtTA transactivator. The Harbour HCAb 2.1 mice expressing HCAbs with fully human VHs without mouse endogenous antibodies were crossed with HNRPA2B1/rtTA2^{S}-M2 transgenic line 9 mice for this purpose (Katsantoni et al., 2007) and bred to homozygosity. The injected oocytes were transferred into pseudo-pregnant B6CBAF1/JRj mice (20–25 per female mouse) (Nagy et al., 2003). The human MSLN transgene was detected in the progeny by polymerase chain reaction (PCR) conducted on DNA samples from the toes using the following primers: Meso s: 5′-GTACCATGGCCTTGCAACGGCTCG and Meso as: 5′-CATCTCGAGTCAGGCCAGGGTGGAGGCTAGG. The mouse lines HCAb 2.1/rtTA2/MSLN-1 and HCAb 2.1/rtTA2/MSLN-3 were both used for inducible immunizations.

2.2 Doxycycline-inducible immunization

Mouse lines HCAb 2.1/rtTA2/MSLN-1 and HCAb 2.1/rtTA2/MSLN-3 were generated and immunized according to the license **AVD101002016512** approved by the Dutch CCD (Central Ethical Committee for Animal Experimentation) under the generation study plan **16-512-09,** with approved changes to the study plan **16-512-03** for doxycycline immunization.

In short, the experimental group consisted of 10 mice including both MSLN lines 1 and 3 in the HCAb 2.1/HNRPA2B1/rtTA2^{S}-M2 background. The mice were given 2 mg/mL doxycycline (doxycycline hydrochloride, Sigma) in drinking water containing 5% sucrose *ad libitum* for 2 days, followed by 2 weeks of drinking water without doxycycline. The bottles were protected from light using aluminum foil to prevent doxycycline degradation. This treatment regimen was repeated six times. Blood samples were obtained before the start of the experiment and after the fourth and sixth induction periods from the submandibular vein; MSLN-specific ELISA was performed on the serially diluted plasma. Two mice with positive titers (saturated signal at dilution 1:1000) were euthanized, and their lymph nodes were dissected to prepare the HCAb library, as described previously (Drabek et al., 2022). A schematic of this process is depicted in Figure 1.

2.3 HCAb library preparation

In brief, the total RNA and cDNA were prepared from a single suspension of lymphoid cells from the dissected lymph nodes without any selection step. The human variable regions were amplified, and the HCAb library was created as described previously (Drabek et al., 2022). The reference details all protocols along with all the materials and methods necessary to obtain human HCAbs from the Harbour HCAb mice through bacterial and eukaryotic libraries of the VH repertoires. In short, the VHs were cloned as PVU II/BSTEII fragments into eukaryotic pCAG hygro hIgG1 vector, and the bacterial library was created by transfection into *E. coli* Mega X DH10B T1 electrocompetent cells.

Approximately 2,000 individual colonies were picked, grown overnight at 37°C in TB medium, and individual plasmids were isolated. This was followed by transient transfection of HEK 293T cells in 96-well format and testing of the supernatants 48 h later in an antigen-specific ELISA using his-tagged MSLN (296–580) ECD (ACRO) coated on the ELISA plates and cell based ELISA using COV644 cells (expressing human MSLN) grown in 96-well plates or through flow cytometry analysis.

2.4 Antigen and cell based ELISA

The plates were coated with 5 μg/mL of his-tagged human MSLN (MSN-H5223, ACRO Biosystems) in phosphate-buffered saline (PBS) overnight at 4°C. For the cell-based ELISA, the cells expressing human MSLN were seeded in 96-well plates on the day before the experiment. The following steps were then identical; however, the volumes differ depending on the format of the ELISA (384- or 96-well plate as reported previously). After blocking for 30 min at room temperature (RT) in a blocking solution (1% milk/1% bovine serum albumin (BSA) in PBS), approximately 50 μL of the individual supernatants was added to the wells and incubated for 2 h at RT. After washing thrice with PBS/0.05% Tween, the plates were incubated with a secondary antibody, i.e., rabbit anti-human IgG-HRP (1:2,000) for 1 h at RT (15 or 50 μL depending on the ELISA plate format), washed in a similar manner as reported previously, and exposed to the BM blue POD substrate (15 or 50 μL) for 5–10 min. The reaction was blocked by adding 20 μL of 1 M H_2SO_4, and the OD was measured on an ELISA reader at 450 nm.

2.5 HCAb production

The pCAG hygro19G6hG1 adherent HEK 293T cell clone obtained from the original HCAb library was expanded in DMEM (BioWhittaker Lonza cat no. BE12-604F/41)/10% fetal calf serum (FCS; BioWhittaker)/NEAA (BioWhittaker Lonza cat no. BE13-114E)/PEN/Strep (Sigma 070M0765) and hygromycin at 200 μg/mL (Hygromycin B, Roche Diagnostics GmbH, REF10843555001). The cells were expanded to 14-cm dishes, carefully washed with PBS, with medium change to 20–25 mL of serum-free medium per dish (Optimem +GlutaMax TK-I (Gibco, 500 mL, 51985)/NEAA/PEN/STREP/Hygro. The production medium was collected twice weekly and replaced, spun in 50-mL tubes (Greiner Bio one Cellstar tubes Cat No 227261) for 5 min at 1800×*g*, transferred to new tubes, and antibody purified using protA beads (Protein A-Agarose Fast Flow, SIGMA P3476-5 mL) on a homemade column. The samples were washed with PBS and eluted with 3 M KSCN, and the buffer was exchanged to PBS using an Amicon 30 kDa spin filter.

For the radiolabeling studies and *in vivo* experiment, 19G6 was cloned into the pCAG hygro hG2 vector and antibody produced by a commercial vendor U-ProteinExpress BV (Utrecht, Netherlands).

All buffers used herein were prepared using Versylene (endotoxin-free and sterile) water. The endotoxins were removed from the glasswork, QuixStand, Äkta-explorer by incubation with 0.1 M NaOH for at least 16 h. Line clearance was performed at the start and end of production. The HEK 293E-253 cells were transfected with endotoxin-free plasmid DNA. Six days post transfection, the conditioned medium containing recombinant antibodies was harvested using SartoClear Dynamics. A 100 μL sample was obtained and stored at 4°C. The antibody was bound batchwise to 2 mL MabSelectSure LX for 4–5 h, and the MabSelectSure LX sepharose-containing bound antibody was harvested by centrifugation before being transferred to a gravity flow column. Non-specific bound proteins were removed by washing the column sequentially with PBS, PBS containing 1 M NaCl, and PBS. The bound antibodies were eluted using 100 mM citrate at pH=3.5, and 5-mL fractions were collected in 12-mL tubes containing 4 mL of 1 M Tris at pH=8.0 for neutralization to pH=7. The protein-containing fractions were pooled, and the MabSelectSure LX pool was concentrated to 2–3 mL using an Amicon 30 kDa spin filter. The aggregates in the concentrated pool were removed by centrifugation, and the concentrated sample was stored at 4°C before gel filtration using a Superdex 200 16/600 column equilibrated in PBS. The protein-containing fractions were analyzed by LabChip capillary electrophoresis, and the recombinant-antibody-containing fractions were pooled and filter-sterilized using a 0.22-μm syringe filter. The resulting product was stored in 1-mL aliquots at 4°C and analyzed by LabChip capillary electrophoresis.

2.6 Affinity measurements

The MSLN protein (296–580) ECD (ACRO) was biotinylated with EZ-Link Sulfo-NHS-Biotin sulfosuccinimidobiotin (Thermo Fischer Scientific) dissolved in dimethyl sulfoxide (DMSO; 1.0 g/L) according to the manufacturer's instructions. The affinity measurements were performed on an Octet red 96 (ForteBio) instrument. Streptavidin biosensors (ForteBio, Sartorius) were used for loading the biotinylated MSLN, and binding assays were performed at 30°C with agitation at 900 rpm and PBS buffer (200 μL per well) in black 96-well plates (Costar). After equilibration of the sensors for 5 min in PBS, the ligand was loaded (5 min), followed by baseline (2 min), association with the analyte (10 min), and dissociation (10 min). The 19G6 HCAb was used as an analyte in concentrations ranging from 20 nM to 1.25 nM. The data analysis and curve fitting were done using Octet software 10.0, and the standard deviation was calculated.

2.7 Cell lines and culture conditions

NIH OVCAR-3 cells (ATCC, Manassas, VA, United States) were maintained in RPMI-1640 medium (Gibco, Invitrogen, Breda, Netherlands) supplemented with 20% FCS (HyClone, Celbio, Logan, UT, United States), 2 mM glutamine (Sigma-Aldrich, St. Louis, MO, United States), 10 mM HEPES (Sigma-Aldrich), 1 mM pyruvate (Sigma-Aldrich), and 0.01 mg/mL insulin (Merck, Sigma-Aldrich). The COV644 human ovarian epithelial-mucinous carcinoma cell line (Sigma®; St. Louis, MO, United States) was cultured in DMEM with 2 mM glutamine and 10% FCS. The HEK 293T (ATCC, CRL-3216) and CHO-K1 (ATCC, CCL-61) cells were cultured in the same medium and used as a negative control (not expressing human MSLN). The COV413A (Merck 07071905), HOC7 (CVCL_5455),

HELA (ATCC, CRM-CCL2), CAPAN2 (ATCC, HTB-80), PANC1 (ATCC, CRL-1469), and A549 (ATCC, CCL-185) lines were used to asses binding of the selected anti-MSLN antibody and their surface expressions of MSLN.

All cell lines were maintained in a humidified 5% CO_2 atmosphere at 37°C.

2.8 Flow cytometric analysis of HCAbs binding to cell surface MSLN

Cells for the flow cytometry analysis were removed from the plate with non-enzymatic cell dissociation solution (C5789, Sigma-Aldrich), washed, and resuspended in cold PBS with 0.5% BSA. The antibodies were bound to the cells in 96-well round-bottom plates and incubated on ice for 30 min. After washing with PBS containing 0.5% BSA, the bound antibodies were detected by incubation with goat pAb anti-human IgG DyLight 488 (ab97003, ABCAM) at 1:200 dilution. Titration of the antibody binding was done on the COV644 cells. To show exclusive binding of the membrane-bound MSLN, sMSLN (MSN-H5223, ACROBiosystems) was added to the incubation mixture in a 1:4 M ratio to HCAbs or the amatuximab control antibody. Binding to the cells was measured using a Fortessa FACS (BD biosciences), and the data were analyzed using FlowJo_ v10.8.1 software. The reference antibody amatuximab was purchased from Creative Biolabs as unconjugated, Fc unmodified mouse/human IgG1 chimera, with 95% SDS purity (CAT#TAB-201).

2.9 DTPA-conjugation of 19G6

Buffer exchange was performed by applying 1.5 mL of 19G6 (8.3 mg/mL) to a gel filtration column (disposable PD-10 desalting column, GE Healthcare Life Sciences, Diegem, Belgium) with the addition of 1 mL of Na_2CO_3 (50 mM, pH 8.5) buffer. The gravity protocol was used according to the manufacturer's instructions, and the antibody was eluted with 3 mL Na_2CO_3 buffer. Conjugation with p-SCN-Bn-DTPA (B-305, Macrocyclics Inc., Plano, TX, United States) was performed by adding a 6-fold molar excess of p-SCN-Bn-DTPA. A stock solution of p-SCN-Bn-DTPA was prepared in DMSO with a final concentration of 9.53 mg/mL; then, 64 μL (equal to approximately 609 μg) of this solution was added to the buffer-exchanged antibody and incubated for 1 h at RT with constant stirring. The conjugation mixture was purified on two parallel PD-10 columns as described above using PBS as the exchange buffer. The conjugated antibody was eluted with 2 mL of PBS from each column, the eluates from both PD-10 columns were combined, and the purity was measured by size-exclusion high-performance liquid chromatography (HPLC) with a Phenomenex BioSep 5 μM SEC-s3000 290 Å column (7.8 × 300 mm, 5.0 μm, PN: 00H-2146-K0, Phenomenex, Woerden, Netherlands) with Phenomenex SecurityGuard GFC 3000.

2.10 Radiolabeling

The DTPA-conjugated 19G6 (2 mL of 2.3 mg/mL) was radiolabeled with Indium (^{111}In, Curium, Petten, Netherlands) after adding a two-fold volume of 2-(N-morpholino) ethanesulfonic acid (0.5 M MES, pH=5.5; Sigma-Aldrich, St. Louis, MO, United States) buffer. After incubation for 30 min at RT, 50 mM of EDTA (Sigma-Aldrich) was added to obtain a final concentration of 5 mM. Radiochemical purities for both radiolabeling experiments were determined by instant thin-layer chromatography on silica-gel chromatography strips (ITLC-SG, Agilent Technologies, Santa Clara, CA, United States) in 0.1 M sodium citrate buffer (Sigma-Aldrich, St. Louis, MO, United States), and these values varied between 95% and 97%.

2.11 Internalization kinetics

The internalization kinetics of the ^{111}In-DTPA-19G6 was determined through an internalization assay using NIH OVCAR-3 cells. Two days prior to the experiments, 0.6×10^6 cells/well were plated in 6-well plates. The cells were washed with PBS and incubated at 37°C with 50,000 cpm of the tracer. An excess of unlabeled DTPA-19G6 (2 μg) was added to determine non-specific binding. At 1, 2, 4, and 24 h after incubation, the cells were washed twice with ice-cold binding buffer (RPMI-1640, supplemented with 0.5% BSA). Subsequently, the cells were incubated for 10 min at 0°C in an acid buffer (0.1 M acetic acid, 154 mM NaCl, pH=2.6) to determine the surface-bound fraction. The cells were then washed twice with ice-cold binding buffer to remove all surface-bound tracer from the cells. The cells were removed from the plate using 0.1 M NaOH, representing the internalized fraction. The receptor-bound fraction and cell-associated activity were measured using a gamma counter, together with three standards.

2.12 Animal studies in nude mice

The animal studies were approved by the Nijmegen Medical Center Animal Ethics Committee (RUDEC) and Dutch Animal Ethics Committee (CCD) of Radboud University and were conducted in accordance with the Institute of Laboratory Animal Research Guidelines. The mice were housed in a pathogen-free environment in Mouse IVC Blue line cages (five mice per cage) with *ad libitum* access to water and chow; they were allowed to adapt to laboratory conditions for at least 1 week before commencing experiments.

The animals were female BALB/cRJ nu mice (Janvier, Saint-Berthevin, France) (6–8 weeks old) and were injected subcutaneously with 10×10^6 NIH OVCAR-3 cells in 200 μL of 1:1 RPMI: Matrigel (VWR International B.V., Amsterdam, Netherlands) in the right flank. After approximately 4–6 weeks, the mice were included in the experiments.

The mouse study no. 2020-007-0370 for optimal time point with ^{111}In-DTPA-19G6 was performed as follows: the female BALB/cRJ nu mice were injected intravenously with 200 μL of 0.45 nmol ^{111}In-DTPA-19G6 containing 10.1–10.7 MBq (SPECT, n=2) or 0.9–1 MBq (biodistribution, n=4). The SPECT animals were scanned for 30 min (4 h post injection), 40 min (48 h post injection), and 1 h (72 h post injection) on a U-SPECTII/CT device (MILabs, Utrecht, Netherlands). For the mice specificity study no. 2020-0007-074, the female BALB/cRJ nu mice (n=5) were injected intravenously with 0.04 nmol ^{111}In-DTPA-19G6

(18.5–18.9 MBq in 200 μL) as a slow bolus. To determine receptor-mediated uptake, a separate group of mice (n=3) was injected with (17.7–17.9 MBq) ^{111}In-DTPA-19G6 together with 4 nmol of unlabeled DTPA-19G6. The SPECT animals were scanned for 30 min (72 h post injection) and 45 min (96 h post injection) on a U-SPECTII/CT device (MILabs, Utrecht, Netherlands).

At the end of each study, the mice were euthanized by CO_2/O_2 asphyxiation; they were then dissected, and the organs were weighed and measured in a γ-counter (Wizard-2480, Perkin Elmer, Boston, MA, United States). The data were statistically analyzed and represented as a mean value per organ/tissue with standard deviation (SD) as the square root of the variance for a measure of dispersion for each dataset. The tumors (and muscles) were fixed in formalin and embedded in paraffin for histological evaluations.

2.13 SPECT

Scans were acquired under general anesthesia (isoflurane/O_2) using the mouse HS 1.0 mm pinhole collimator (U-SPECTII/CT) or GP-M 0.60 mm pinhole collimator (U-SPECT6/CT), followed by a CT scan (U-SPECTII/CT: spatial resolution 160 μm, 65 kV, 0.615 mA or U-SPECT6/CT: spatial resolution 100 μM, 50 kV, 0.4 mA). The scans were reconstructed with MILabs reconstruction software using 16 subsets, with a voxel size of 0.2 mm^3 and one iteration (U-SPECT-II) or using an ordered-subset expectation-maximization algorithm, with a voxel size of 0.4 mm^3, four iterations, and a Gaussian filter of 0.6 mm (U-SPECT-6). Inveon Research Workplace (Preclinical Solutions, Siemens Medical Solutions, Inc., Knoxville, TN, United States) or VivoQuant (Invicro, MA, United States) were used to create the images.

2.14 PET

The scans were acquired under general anesthesia (isoflurane/O_2) on an IRIS PET/CT (Inviscan, Strasbourg, France) and were followed by a CT scan for anatomic reference (spatial resolution of 160 μm, 80 kV). The images were then reconstructed using the 3D-OSEM-MC algorithm (matrix based on Monte Carlo simulation), with eight subsets and eight iterations as well as a voxel size of 0.855 × 0.855 × 0.855 mm on an OsiriX MD (PIXMEO SARL, Geneva, Switzerland).

3 Results

3.1 Generation and immunization of genetically modified Harbour HCAb mice

To raise the human HCAb to human MSLN, Harbour HCAb mice were modified by crossing with transgenic mice ubiquitously expressing the rtTA2^s-M2 transactivator (Katsantoni et al., 2007). They were further modified by injecting fertilized eggs with a human MSLN gene containing a tetracycline-responsive element (TRE) (seven repeats of TetO separated by spacer) placed upstream of a minimal CMV promoter driving expression of human MSLN (Nagy et al., 2003). After obtaining a number of founders, two gave germ-line transmission and were used to establish the new genetically modified (GM) lines. None of the tested progeny showed human MSLN in the uninduced state, indicating that there was no leakiness in the system. Leaky expression would cause tolerance toward human MSLN and prevent immune responses, i.e., antibody production. Five mice of each line were used for immunization. Six-week-old transgenic mice were induced six times at 2-week intervals to provide a pulse of human MSLN protein expression (Figure 1). The anti-MSLN titers in their blood were measured after the fourth round of induction. Two mice (one of each line) showed satisfactory titers against human MSLN; they were orally induced with doxycycline two more times and euthanized.

3.2 HCAb selection

The lymph node cells were collected and HCAbs were isolated by our standard procedure (Drabek et al., 2022). Approximately 2,000 HCAbs were expressed in the HEK 293T cells and their supernatants when tested 48 h later for the presence of anti-MSLN antibodies using MSLN-specific ELISA and cell-based ELISA. A total of 110 positive supernatants were obtained in a regular protein ELISA, of which 28 were positive in the COV644 cell-based ELISA; these were confirmed by flow cytometry on the COV644 cells. Titration of antibody binding was performed, and EC50 was determined (Supplementary Figure S1). The corresponding plasmids were sequenced to exclude identical clones, which reduced the total number to 14 HCAbs with unique VH sequences. Number of these show high similarity in the CDR3 region, which corresponded with their ability to bind MSLN on the cell surface. The 7F8, 9E4, 19G6, 20B8, and 51 8-10 antibodies bind preferentially to the surface MSLN on the COV644 cells (Figure 2A), while 2E12, 7D7-1, 11A10, 14A8, 14E8, and 17F6 bind sMSLN, as shown by adding sMSLN in excess to the cell-surface binding assay (similar to that observed for the reference antibody amatuximab). The 19G6 HCAb was selected based on its binding characteristics that originated from the IGHV3-73 human germline with four extra somatic hypermutations and 12-amino-acid-long CDR3 region (Supplementary Figure S2, accession number PP861029). We tested 19G6 on different human cancer cell lines, namely COV644, COV413A, HOC7, HELA, CAPAN2, PANC1, and A549, using HEK 293T (human embryonic kidney cell line) and CHO (hamster ovarian cell line) as the negative controls (Supplementary Figure S3). The binding was in accordance with the expression data reported (proteinatlas.org/ENSG00000102854-MSLN/cell+line). We also tested the binding of 19G6 to OVCAR-3 cells because these were chosen for the *in vivo* xenotransplantation model in mice. Comparison with amatuximab showed that 19G6 had a similar affinity when compared to the 1.5 nM reported for amatuximab (Hassan et al., 2007) and achieved binding at a lower range of concentrations than the reference antibody (Figure 2B). This may be because amatuximab binds the same epitope of MSLN with which it binds Mucin-16, which is present in high concentrations on the surface of the OVCAR-3 cells (https://

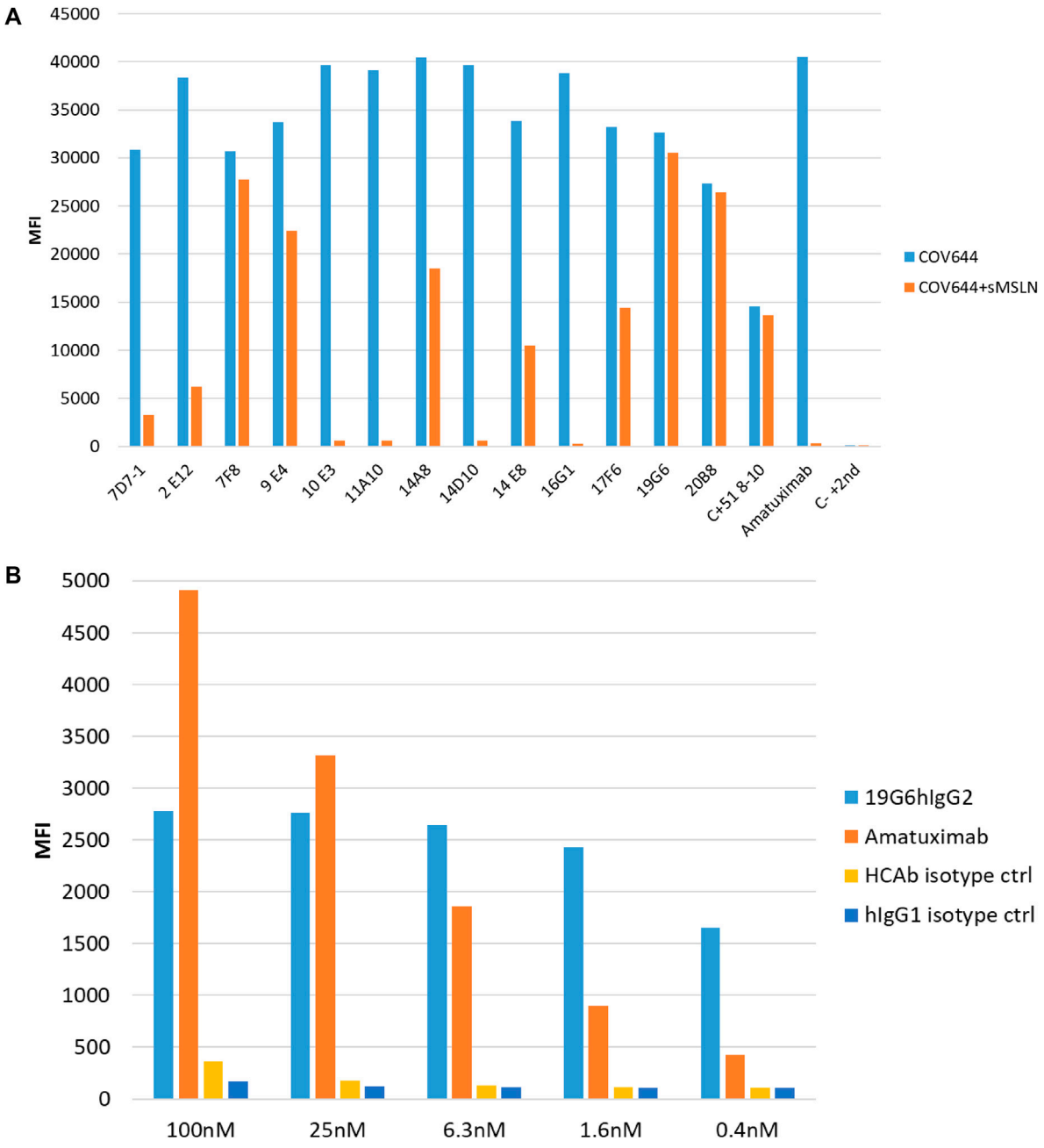

FIGURE 2
(A) Binding of selected HCAbs to MSLN expressed on the COV644 cell membrane in the absence (blue bar) or presence (orange bar) of soluble MSLN by flow cytometry. **(B)** Binding on OVCAR-3 cells with decreasing concentrations of amatuximab and 19G6. Irrelevant isotype controls were used for both antibody formats.

www.proteinatlas.org), whereas 19G6 does not share this epitope. On the basis of binding to the cell-surface MSLN and affinity of 1.65 ± 0.23 nM (Figure 3), we selected HCAb 19G6 for further experiments.

For the *in vivo* imaging in the mouse xenotransplantation study (see below), we exchanged the original human IgG1 backbone with human IgG2 based on the properties of human IgG subclasses binding to human and mouse Fc receptors (Vidarsson et al., 2014; Dekkers et al., 2017). Human IgG2 has been reported to bind only to mouse FcγRIIb and FcγRIII, with a similar reactivity pattern as mouse IgG1, albeit with a 5–60 times lower affinity, while it does not bind to FcγRI, FcγRIIb/c, FcγRIIIa F158, and FcγRIIIb in humans. The isotype change was achieved by recloning the 19G6 VH (Supplementary Figure S1, accession number PP861029) into a pCAG hygro G2 vector (Drabek et al., 2016).

3.3 Internalization and Lindmo assay on OVCAR-3 cells

The labeling efficiency of ^{111}In-DTPA-19G6 was >96%. After 1 h, 12.7 ± 1.7% of the added ^{111}In-DTPA-19G6 was bound to the

10.3389/fchbi.2024.1408621

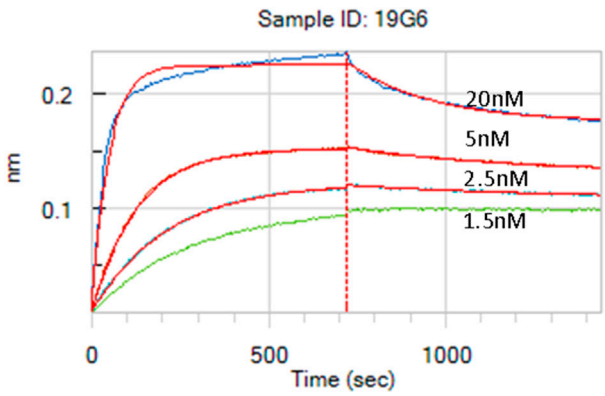

FIGURE 3
Affinity measurement of 19G6 using the biolayer interferometry (BLI) Octet system. The calculated KD is 1.65 nM, with a standard deviation (SD) of 0.23 nM.

cells, which increased to 26.8 ± 0.5% after 24 h. The internalized fraction was low at 0.5 ± 0.1% at 1 h but increased substantially to 18.1 ± 0.7% after 24 h. In the presence of excess unlabeled DTPA-19G6, both the binding and internalization reduced to <1%, indicative of receptor-specific binding of ^{111}In-DTPA-19G6. Thus, ^{111}In-DTPA-19G6 shows excellent receptor-mediated binding to and internalization in NIH OVCAR-3 cells (Figure 4).

Next, a Lindmo assay was performed, and the labeling efficiency was 88%, as determined by ITLC. After purification, the radiochemical purity was >98%. The ^{111}In-DTPA-19G6 was stable over 6 h in PBS at RT. Thus, the compound was stable until at least the time of injection (Supplementary Table S1). An immunoreactive fraction of 79% was calculated, and the data were plotted in a binding plot (specific cell-bound activity/total applied activity *versus* cell concentration) and Lindmo plot (total applied activity/specific cell-bound activity *versus* inverse cell concentration). The immunoreactive fraction was calculated from the *y*-axis intercept using GraphPad Prism software (Figures 5A, B). After labeling, the conjugate was still highly immunoreactive.

3.4 *In vivo* xenotransplantation experiments in BALB/cRJ nu mice

For the *in vivo* experiments in BALB/cRJ nu mice, SEC-FLPC was performed 2 h and 24 h after radiolabeling. The first preparation showed 5% aggregates, 85% 19G6, and 10% lower molecular mass peaks, while the second preparation showed 2.5% aggregates, 82.5% 19G6, and 15% lower molecular mass peaks. The SEC-FLPC reports are deposited as Supplementary Material.

A total of 18 mice were inoculated subcutaneously with 10×10^6 NIH OVCAR-3 cells in Matrigel. The tumors grew over a 4-week period, following which the mice were injected intravenously with ^{111}In-DTPA-19G6, i.e., 0.45 nmol equal to 1 MBq (diluted with PBS/0.5% BSA per mouse) for the biodistribution study. At each time point (4 h, 48 h, and 72 h post injection) four mice were euthanized, and 11 different organs/tissues were dissected (Figure 6).

The average distribution of radioactive labels is shown in Figure 6A (the pancreas was removed only at the 72-h point). The biodistribution after dissection showed increasing tumor accumulation of 19G6 from 4.9 ± 1.2% ID/g at 4 h post injection to 15.6 ± 2.4% ID/g at 48 h, which remained at 15.5 ± 2.6% ID/g at 72 h, indicating good tumor retention over time. Blood clearance was slow, with 12.9 ± 0.7% ID/g at 4 h post injection decreasing to 6.4 ± 0.2% ID/g at 48 h and 3.7 ± 1.4% ID/g at 72 h. The initial uptake in the liver was high (26.7 ± 1.9% ID/g at 4 h) but decreased to 8.8 ± 0.8% ID/g at 48 h and 5.5 ± 2.0% ID/g at 72 h. The kidney uptake was stable over all time points (6.7 ± 0.1% ID/g (4 h); 7.2 ± 0.4% ID/g (48 h); 5.5 ± 0.4% ID/g (72 h)). Accumulation in all other

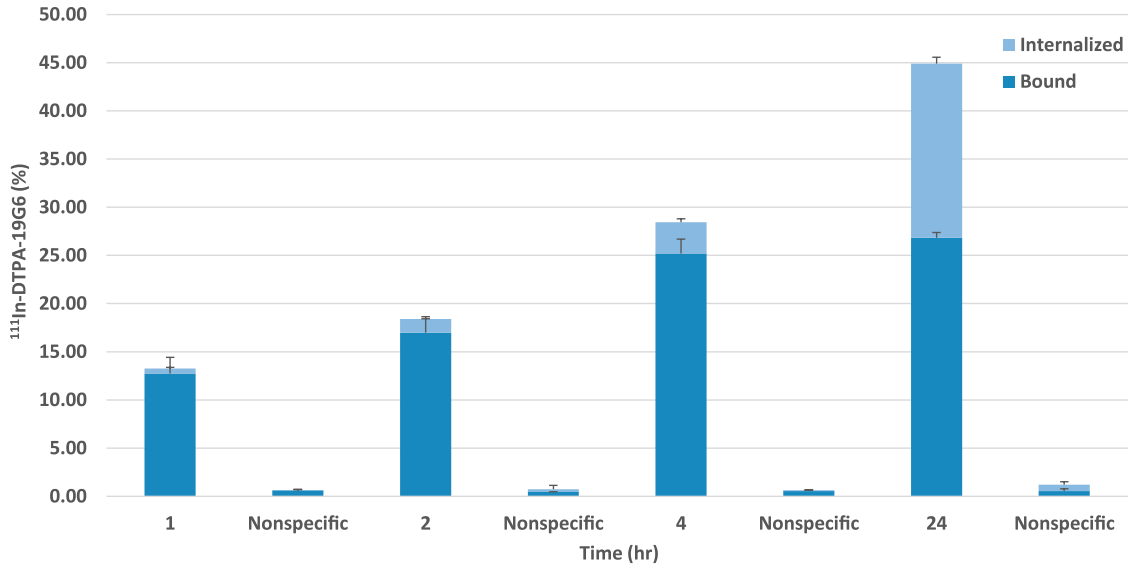

FIGURE 4
Binding and internalization kinetics of ^{111}In-DTPA-19G6 on NIH OVCAR-3 cells. Cell-bound (dark blue) and internalized fractions (light blue) are presented. Non-specific binding and internalization were determined by co-incubation with an excess of unlabeled DTPA-19G6.

10.3389/fchbi.2024.1408621

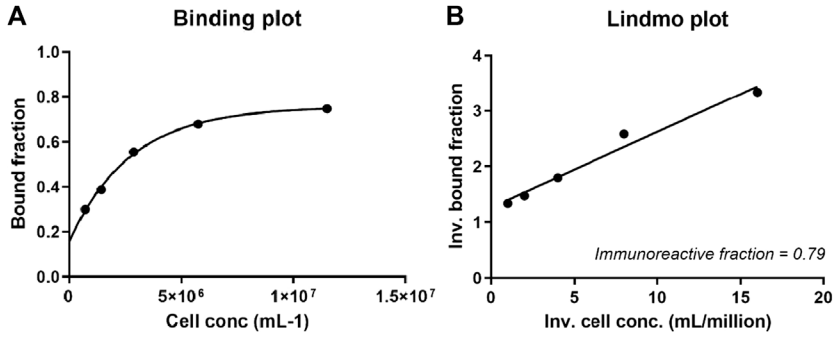

FIGURE 5
(A) Binding and **(B)** Lindmo plots of ^{111}In-DTPA-19G6 on NIH OVCAR-3 cells. The immunoreactive fraction is 79%.

organs was low. For the SPECT analysis, the mice received 45 nmol of the radiolabel equal to 10 MBq (diluted with PBS/0.5% BSA) per mouse, and two mice were scanned at each time point. The SPECT images confirmed the biodistribution data obtained after dissection (Figures 6B, 7, Supplemental Movies S1–S3). Some accumulation of the radiolabel was observed in the SPECT images around the neck area (Supplemental Movies S1–S3 for the three time points). Further investigations showed uptake by the salivary glands, which were also dissected in the second experiment for the biodistribution study. We concluded that the *in vivo* targeting was almost completely tumor-specific and that the images should be acquired at least 72 h after injecting the radiolabeled antibody or even later.

Next, a second *in vivo* experiment was carried out to confirm the tumor specificity of 19G6 binding. To this end, the mice were inoculated subcutaneously with 10×10^6 NIH OVCAR-3 cells in Matrigel, and the tumor was grown for a period of 7 weeks. Five mice were injected intravenously with 10 × less-radioactive label (0.04 nmol approximately equal to 8 MBq of ^{111}In-19G6 diluted with PBS/0.5% BSA per mouse). A separate group of three mice were injected with the same amount of radiolabeled antibody with the addition of 4 nmol of non-radiolabeled DTPA-conjugated antibody (100-fold excess). SPECT scans were then acquired at 72 and 94 h post injection, and a biodistribution assay was performed on a broader range of organs 96 h post injection (Figure 8A). The uptake of ^{111}In in the NIH OVCAR-3 tumor was 18.9 ± 10.5% ID/g in the first five mice, but the accumulation in the tumor reduced to 3.3 ± 0.3% ID/g in the three mice that were co-injected with excess unlabeled 19G6 (Figure 5A). The SPECT images after injection of ^{111}In-DTPA-19G6 showed accumulation in the tumor and also the liver. Blocking the labeled 19G6 with an excess of unlabeled 19G6 resulted in non-detectable tumor uptake in the SPECT images, whereas liver accumulation was not affected by the excess of unlabeled 19G6, confirming that the binding of 19G6 is tumor-specific (Figures 8B, C).

4 Discussion

A novel HCAb was developed using *in vivo* induction of the antigen using a transgenic approach and oral doxycycline-induced expression of the target antigen. Thus, the injection of an antigen (protein, peptide, cells, DNA, and RNA) was replaced by drinking water containing doxycycline. This approach has the advantage that antibodies can effectively be raised against "difficult antigens", these being those that are difficult to produce in *in vitro* expression systems available; those that are surface markers or parts of the complexes expressed on the surfaces that have to be presented to the immune system in their natural conformations; those containing non-immunodominant target epitopes; and those whose epitopes are slightly different between the human and mouse homologs. For this study, we used a well-characterized mouse line in which the methylation-free CpG island of the human housekeeping hnRNPA2B1-CBX3 gene locus is capable of driving expression of a linked rtTA2S-M2 transgene in the mice in all tissues examined. The generation of the new HCAb lines containing the target transgene of interest (MSLN) linked to a TRE containing tetracycline sequences resulted in two new GM mouse lines. Although the efficiency of the tet system in transgenic animals is often negatively impacted by the chromosomal site of integration, both of the newly generated HCAb lines did not express MSLN in the uninduced state and only expressed it upon doxycycline induction. We tested the system with several other targets, which showed that the number of animals that built sufficient titers of specific antibodies varied and could be related to the dosage of doxycycline that was not strictly controlled, i.e., the animals drink *ad libitum*. The disadvantage of this method is that it requires time-consuming genetic modification of the mice. In this particular application, we bred a founder MSLN mouse to obtain a line and certain numbers of mice for oral induction of antigens (immunization), both of which are time-consuming. This time can be shortened considerably using directly generated founders. These can first be analyzed from the same biopsy used for genotyping and from blood taken at later stages to show that the genes coding for the antigen are silent (at least in the places tested) before induction of the target antigen to raise antibodies. Such a system can be made in cassette form in HCAb/rtTA/TRE target ES cells isolated from these mice that would allow easy and rapid exchange of the target antigen gene. The ES cells can be introduced into blastocysts to generate chimeric founder mice, which could be immunized given that the presence of modified cells in the chimeras would be sufficient for induction of immunization, thereby obviating the need for breeding. Alternatively, and perhaps even faster, would be exchanging old for

10.3389/fchbi.2024.1408621

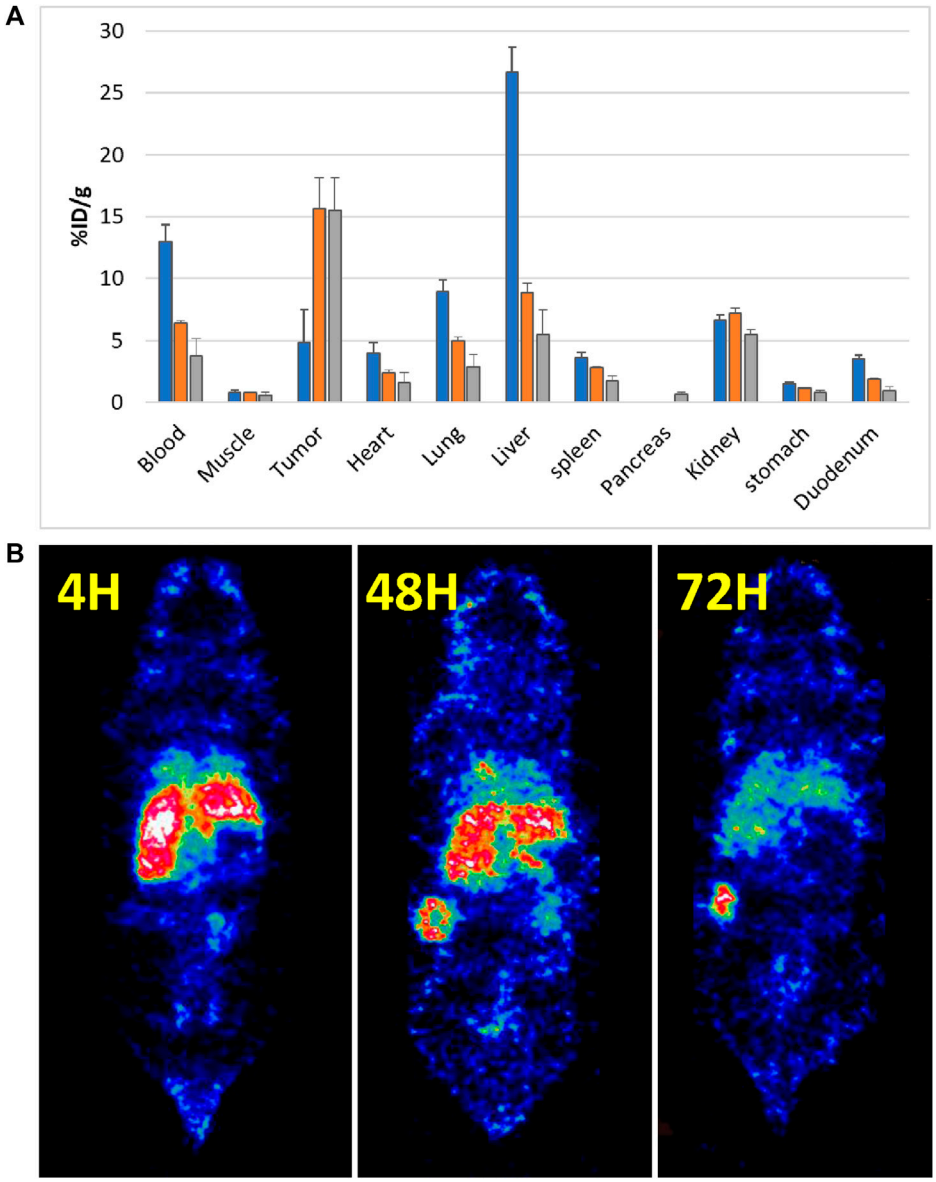

FIGURE 6
^{111}In-labeled 19G6 accumulation in experimental animals after 4, 48, and 72 h post intravenous injection: **(A)** average biodistribution (per four animals) after 4 h (blue bar), 48 h (orange bar), and 72 h (gray bar); **(B)** SPECT images acquired at the same time points showing accumulation of the label in the tumor after 48 h. The non-specific label uptake in the liver and spleen start disappearing at 72 h post injection.

novel antigens in the fertilized eggs using Crispr/Cas9 (using the mice described herein) and using these offspring for immunization. Exchanging antigens through either procedure using the current mice would guarantee that the exchanged antigen is silent before induction and only expressed after induction.

HCAb 19G6 is an interesting antibody as it is smaller than normal H2L2 antibodies, providing better penetration of the tumor/tissue and specific binding to the membrane-bound form of MSLN as opposed to most anti-MSLN antibodies that (also) bind sMSLN shed from the tumor. The presence of sMSLN causes several problems for visualization. First, more antibody is needed to visualize the tumor because sMSLN "soaks" up a lot of antibody and thereby causes a background signal throughout circulation. It is not yet clear which epitope is bound by 19G6, but the data suggest that it is a spatial rather than a linear epitope. The fact that the antibody recognizes soluble his-tagged ECD of MSLN (296–580) when coated on plastic (as in the case of ELISA) and membrane-bound MSLN on different MSLN-positive cell lines (in flow cytometry experiments) suggests that the epitope is not in the C-terminal part of the protein close to the membrane GPI anchor (580–600) that is not present in the ECD domain used. Thus, the epitope is different from the juxtamembrane epitope binding protease-sensitive region (where shedding occurs) by the 15B6 antibody (Liu et al., 2024). Biotinylated ECD of mesothelin, when loaded on streptavidin sensors, binds the antibody in solution, but when the antibody is loaded onto anti-human Fc sensors, it does not bind with ECD of human mesothelin (260–580) in solution. The same

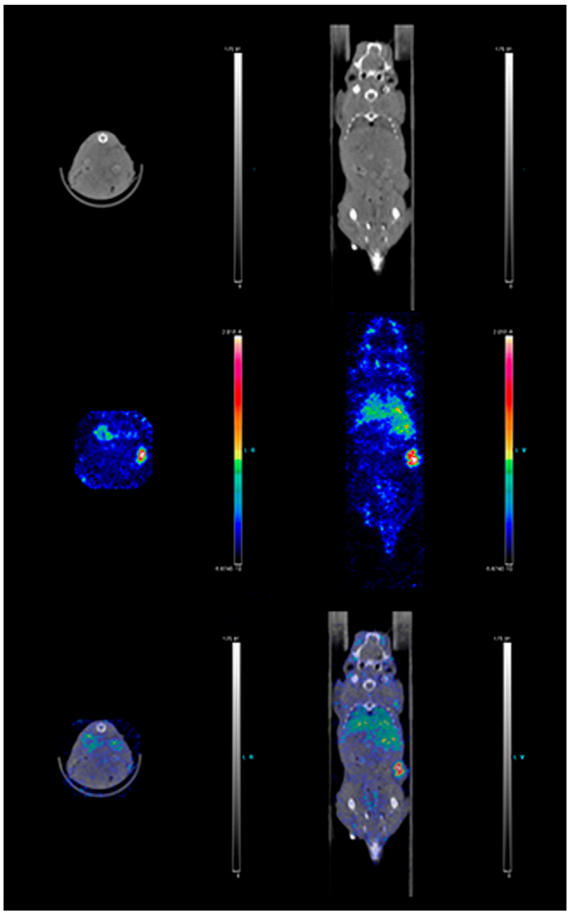

FIGURE 7
Combined SPECT/CT images of a mouse 72 h post injection of ^{111}In-DTPA-19G6. Mouse anatomical details and tumor growth on the right flank are depicted in the top row; the radioactive label accumulation is shown in the middle row; overlay of the two images is shown in the bottom row. The tumor is radioactively labeled (red).

is true for ELISA. The antibody binds to the coated ECD of mesothelin, but binding is prevented when the antibody is coated on the plate; this suggests that the allosteric changes to the protein (when attached to the surface) contribute to the epitope exposure and consequently the binding. To date, crystallization of the truncated MSLN variants and full-length MSLN (fl MSLN 296-600 of the precursor protein) produced in insect cells as soluble proteins (dataset identifier PXD034397, 8CX3) have not been sufficient for prediction owing to the lack of conformational variability necessary for accessibility of the otherwise-occluded epitope. Altogether, 19G6 binds the membrane-associated MSLN on cells, and the epitope appears to be within the canonical sMSLN (residues 296–580) that is exposed when immobilized on the BLI biosensor or ELISA plate.

In the present study, we successfully demonstrate the preclinical SPECT imaging of mesothelin-expressing tumors using radiolabeled HCAb 19G6 using OVCAR-3 cells via a xenotransplantation experiment. Most established cancer cell lines differ in the numbers of mesothelin molecules expressed on the cell surface, which range from more than 1×10^5 to much less, such as OVCAR-3 that has as little as 12,000 MSLN sites per cell (Ho et al., 2011). In the clinic, the detection of early metastasis and determination of local tumor residues after surgical removal of the bulk tumor are rather challenging tasks; we have therefore chosen to image a tumor with a low density of MSLN molecules. For imaging, the half-life of the antibody should be short; thus, smaller formats such as scFv and single-domain antibodies are preferred. However, in PET imaging, scFvs successfully detect cancer cells that express MSNL at high levels but do not detect tumor cells that express mesothelin weakly (Yakushiji et al., 2019). For clinical application of antibodies as imaging reagents, it is also essential to have good penetration while avoiding redundant immune responses and non-specific labeling via Fc receptors. Here, we used the HCAb format that is half the size of a classical tetrameric antibody and is bivalent, while we have shown previously that HCAbs have better penetration in tumors than classical antibodies (Gan et al., 2022). The initial study using 0.4 nmol of radiolabeled antibody per mouse showed that the tumor was not visible 4 h post injection. However, it was clearly visible 2 and 3 days later, when the liver and spleen (organs that initially took up the majority of non-specific labeling) are clearing out the label. Based on this result, we concluded that imaging could even be possible at a later stage. On the rotating images (Supplemental Movies S1–S3), two symmetric dots of labels were detected in the neck/jaw area above the background. After dissecting, these labeled areas were shown to be the salivary glands. Searching through available images from mouse and human subjects in literature shows that this is not uncommon but often never touched upon in the discussion (Ter Weele et al., 2015; Lamberts et al., 2016). This phenomenon was also observed with a PSMA antibody in the treatment of prostate cancer, which in humans causes dose-limiting toxicity and xerostomia. The reasons are not completely clear and are controversial, i.e., is the signal due to PSMA expression in the salivary glands or is it non-specific uptake of the radioactive label by the salivary glands (Mahajan et al., 2022). It was recently shown that such uptake can be blocked by administering either saline or cold antibody drug conjugates or monosodium glutamate and kynurenic acid locally via cannulation or systemically (Roy et al., 2021; Heynickx et al., 2023).

The second animal experiment shows clear tumor specificity since competition with the non-radioactive label in excess prevents accumulation of radioactivity in the tumor. The two experiments in this study were conducted separately with different batches of DTPA-conjugated antibodies, and we used 0.04 nmol of radioactively labeled antibodies for the second study. The SPECT and PET images in the second experiment were obtained 4 days after injection and still show high non-specific backgrounds (liver and spleen). This can be explained by many factors, where even slight differences in the number of DTPA molecules attached per antibody may offer different immunoreactivity and biodistribution. For example, Sakahara and colleagues reported that indium-labeled antibodies containing 5.5 DTPA molecules per antibody showed low tumor accumulation but high liver uptake in comparison to the same antibody with less DTPA molecules attached (Adumeau et al., 2016). This probably reflected the degree of denaturation of the antibody by the heavy conjugation of DTPA, although the investigators did not confirm dimer or polymer complexes by column chromatography (Adumeau et al., 2016). The aggregates or degradation products could explain this. However, the second batch showed only 4%–5% more of the lower molecular size peaks than the first batch. It should be noted that random conjugation via lysines can cause batch-to-batch reproducibility issues. Even if the batches of an immunoconjugate possess the same degree of labeling, it would be quite unlikely that two

10.3389/fchbi.2024.1408621

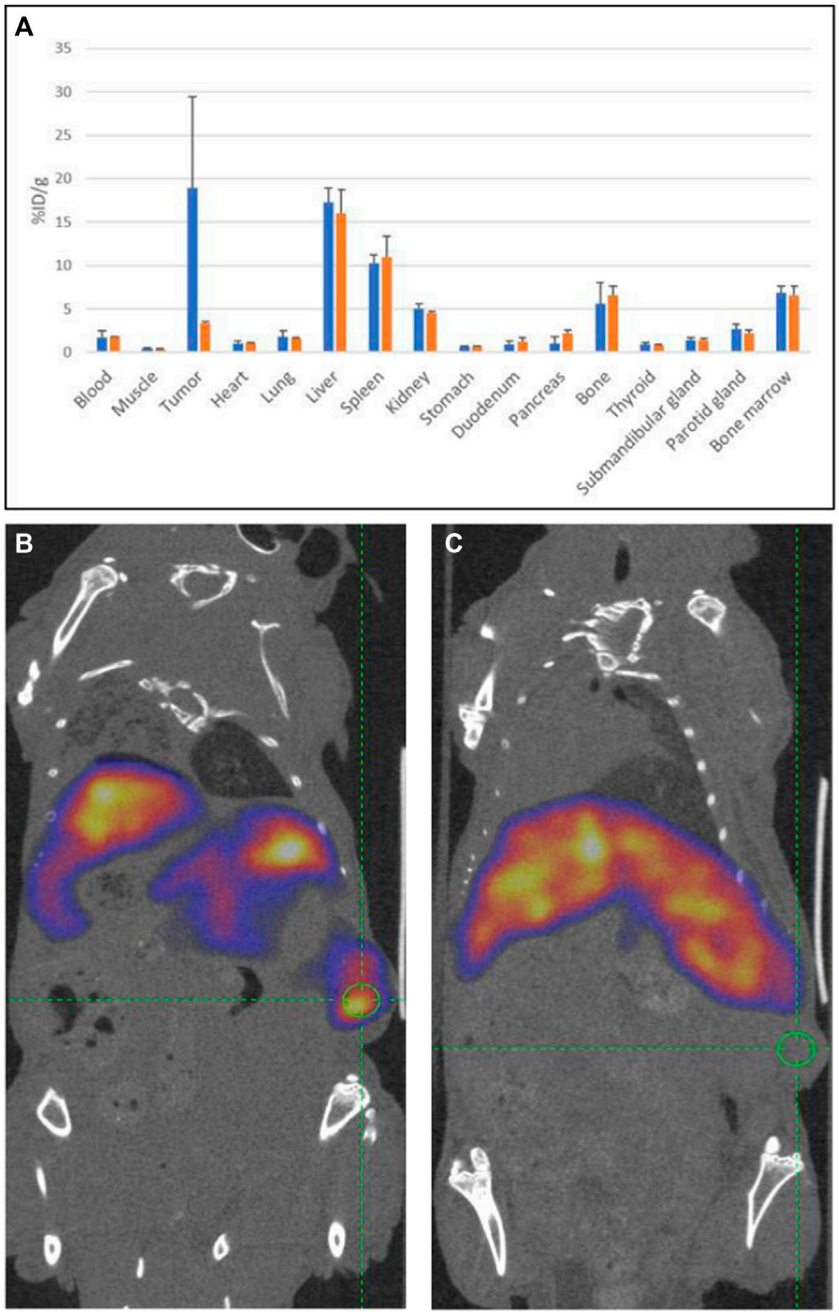

FIGURE 8
Tumor specificity of 19G6: **(A)** average biodistributions of radioactive ^{111}In-labeled 19G6 in experimental animals 96 h post injection (in blue) and radioactive label 96 h after injection of mixture of radiolabeled 19G6 antibodies with 100-fold excess of unlabeled antibodies (in orange). The standard deviation (SD) for each organ dataset is represented as an error bar (in black). SPECT/CT images of animals bearing tumor (green circle) 96 h after injection with **(B)** ^{111}In-DTPA-19G6 and **(C)** ^{111}In-DTPA-19G6-labeled antibodies with 100-fold excess of cold 19G6-DTPA.

batches will have exactly identical mixtures of regioisomers. Each regioisomer has a unique set of chemical, biological, and pharmacological traits, which could lead to decreased accumulation in the target tissue and increased uptake in healthy tissues (Agarwal and Bertozzi, 2015). Thus, every new conjugate must undergo extensive optimization. Such optimization would be required for liver background staining since most tumors overexpressing MSLN metastasize to the liver. Site-specific labeling (via engineered cysteines, sortase, or glycomodification) is an option for improvement (Zhou et al., 2014; Agarwal and Bertozzi, 2015; Beerli et al., 2015), in addition to possible lyophilized formulations of the immune conjugates provided that the integrity and purity of the conjugates remain intact (Ackova et al., 2016).

In conclusion, our novel human anti-MSLN HCAb reacted with MSLN-positive cancer cells *in vitro* and did not bind to soluble mesothelin. The *in vivo* data clearly visualize the MSLN-positive

tumors, which shows the potential of the proposed imaging agent for MSLN-positive tumors. As the smallest recognition unit, heavy-chain variable regions (VH) could be used as target parts for building blocks for CART therapies and other therapeutic entities in the future.

Data availability statement

The original contributions presented in the study are included in the article/Supplementary Material, and any further inquiries may be directed to the corresponding author.

Ethics statement

Ethical approval was not required for the studies on humans in accordance with the local legislation and institutional requirements because only commercially available and established cell lines were used. The animal study was approved by the Dutch CCD (Central Ethical Committee for Animal Experimentation) and local ethics committee of Radboud University and Erasmus Medical Center. The study was conducted in accordance with all local legislations and institutional requirements.

Author contributions

RJ: conceptualization, formal analysis, investigation, and writing–review and editing. RvH: formal analysis, investigation, writing–review and editing, and methodology. MV: investigation and writing–review and editing. AM: writing–review and editing and methodology. JW: writing–review and editing, funding acquisition, and supervision. FG: supervision, writing–review and editing, conceptualization, and writing–original draft. DD: conceptualization, writing–original draft, writing–review and editing, formal analysis, and investigation.

Funding

The author(s) declare that no financial support was received for the research, authorship, and/or publication of this article.

Conflict of interest

RJ, RvH, DD, and FG are investigators from the Department of Cell Biology, Erasmus Medical Center. FG is a consultant to Harbour BioMed. RJ, RvH, DD, and FG are named as inventors on a patent application PCT/CN2024/095555 and EP24178162.4 (filed on 27th of May 2024) covering methods of producing and the sequence of 19G6. JW is the CEO of Harbour Biomed. All authors except AM have a financial interest in Harbour BioMed.

The remaining author declares that the research was conducted in the absence of any commercial or financial relationships that could be construed as a potential conflict of interest.

The author(s) declared that they were an editorial board member of Frontiers at the time of submission. This had no impact on the peer review process and final decision.

Publisher's note

Supplementary material

The Supplementary Material for this article can be found online at: https://www.frontiersin.org/articles/10.3389/fchbi.2024.1408621/full#supplementary-material

SUPPLEMENTARY MOVIE S1
Rotating 3D image of the mouse with the tumor 4 h post injection of ^{111}In-DTPA-19G6. The tumor is not yet visible, while the liver and spleen take up most of the radioactive label.

SUPPLEMENTARY MOVIE S2
Rotating 3D image of the mouse with the tumor 48 h post injection of ^{111}In-DTPA-19G6. The tumor is clearly visible, while the non-specific labels in the liver and spleen start disappearing.

SUPPLEMENTARY MOVIE S3
Rotating 3D image of the mouse with the tumor 72 h post injection of ^{111}In-DTPA-19G6. The tumor is still clearly visible, while the non-specific labels in the liver and spleen are almost cleared out.

References

Ackova, D. G., Smilkov, K., and Janevik-Ivanovska, E. (2016). Physicochemical evaluation of lyophilized formulation of *p*-SCN-bn-DOTA- and *p*-SCN-Bn-DTPA-rituximab for NHL radio immunotherapy. *Iran. J. Pharm. Res.* 15 (3), 295–302. PMID: 27980563; PMCID: PMC5149015.

Adumeau, P., Sharma, S. K., Brent, C., and Zeglis, B. M. (2016). Site-specifically labeled immunoconjugates for molecular imaging—Part 2: peptide tags and unnatural amino acids. *Mol. Imaging Biol.* 18, 153–165. doi:10.1007/s11307-015-0920-y

Agarwal, P., and Bertozzi, C. R. (2015). Site-specific antibody-drug conjugates: the nexus of bioorthogonal chemistry, protein engineering, and drug development. *Bioconjugate Chem.* 26 (2), 176–192. Epub 2015 Jan 30. PMID: 25494884; PMCID: PMC4335810. doi:10.1021/bc5004982

Asgarov, K., Balland, J., Tirole, C., Bouard, A., Mougey, V., Ramos, D., et al. (2017). A new anti-mesothelin antibody targets selectively the membrane-associated form. *MAbs* 9 (3), 567–577. PMID: 28353419; PMCID: PMC5384705. doi:10.1080/19420862.2017.1288770

Awuah, P., Bera, T. K., Folivi, M., Chertov, O., and Pastan, I. (2016). Reduced shedding of surface mesothelin improves efficacy of mesothelin-targeting recombinant immunotoxins. *Mol. Cancer Ther.* 15 (7), 1648–1655. Epub 2016 May 18. PMID: 27196771; PMCID: PMC4936933. doi:10.1158/1535-7163.MCT-15-0863

Beerli, R. R., Hell, T., Merkel, A. S., and Grawunder, U. (2015). Sortase enzyme-mediated generation of site-specifically conjugated antibody drug conjugates with high *in vitro* and *in vivo* potency. *PLoS One* 10 (7), e0131177. PMID: 26132162; PMCID: PMC4488448. doi:10.1371/journal.pone.0131177

Chang, K., Pastan, I., and Willngham, M. C. (1992). Frequent expression of the tumor antigen cak1 in squamous-cell carcinomas. *Int. J. Cancer* 51, 548–554. doi:10.1002/ijc.2910510408

Chen, S. H., Hung, W. C., Wang, P., Paul, C., and Konstantopoulos, K. (2013). Mesothelin binding to ca125/MUC16 promotes pancreatic cancer cell motility and invasion via MMP-7 activation. *Sci. Rep.* 3, 1870. doi:10.1038/srep01870

Dekkers, G., Bentlage, A. E. H., Stegmann, T. C., Howie, H. L., Lissenberg-Thunnissen, S., Zimring, J., et al. (2017). Affinity of human IgG subclasses to mouse Fc gamma receptors. *MAbs* 9 (5), 767–773. Epub 2017 May 2. PMID: 28463043; PMCID: PMC5524164. doi:10.1080/19420862.2017.1323159

Dochez, V., Caillon, H., Vaucel, E., Dimet, J., Winer, N., and Ducarme, G. (2019). Biomarkers and algorithms for diagnosis of ovarian cancer: CA125, HE4, RMI and ROMA, a review. *J. Ovarian Res.* 12 (1), 28. PMID: 30917847; PMCID: PMC6436208. doi:10.1186/s13048-019-0503-7

Drabek, D., Janssens, R., de Boer, E., Rademaker, R., Kloess, J., Skehel, J., et al. (2016). Expression cloning and production of human heavy-chain-only antibodies from murine transgenic plasma cells. *Front. Immunol.* 7 (7), 619. PMID: 28066429; PMCID: PMC5165034. doi:10.3389/fimmu.2016.00619

Drabek, D., Janssens, R., van Haperen, R., and Grosveld, F. (2022) "A transgenic heavy chain IgG mouse platform as a source of high affinity fully human single-domain antibodies for therapeutic applications," in *Series: methods in molecular Biology book: single-domain antibodies protocol.* doi:10.1007/978-1-0716-2075-5_6

Faust, J. R., Hamill, D., Kolb, E. A., Gopalakrishnapillai, A., and Barwe, S. P. (2022). Mesothelin: an immunotherapeutic target beyond solid tumors. *Cancers (Basel)* 14 (6), 1550. PMID: 35326701; PMCID: PMC8946840. doi:10.3390/cancers14061550

Gan, X., Shan, Q., Li, H., Janssens, R., Shen, Y., He, Y., et al. (2022). An anti-CTLA-4 heavy chain-only antibody with enhanced T_{reg} depletion shows excellent preclinical efficacy and safety profile. *Proc. Natl. Acad. Sci. U. S. A.* 119 (32), e2200879119. doi:10.1073/pnas.2200879119

Grasso, L., Jiang, Q., Hassan, R., Nicolaides, N. C., and Kline, J. B. (2023). NAV-003, a bispecific antibody targeting a unique mesothelin epitope and CD3ε with improved cytotoxicity against humoral immunosuppressed tumors. *Eur. J. Immunol.* 53 (8), e2250309. Epub 2023 Jun 20. PMID: 37146241; PMCID: PMC10524251. doi:10.1002/eji.202250309

Gubbels, J. A., Belisle, J., Onda, M., Rancourt, C., Migneault, M., Ho, M., et al. (2006). Mesothelin-MUC16 binding is a high affinity, N-glycan dependent interaction that facilitates peritoneal metastasis of ovarian tumors. *Mol. Cancer* 5, 50. doi:10.1186/1476-4598-5-50

Hassan, R., Ebel, W., Routhier, E. L., Patel, R., Kline, J. B., Zhang, J., et al. (2007). Preclinical evaluation of MORAb-009, a chimeric antibody targeting tumor-associated mesothelin. *Cancer Immun.* 7 (7), 20. PMID: 18088084; PMCID: PMC2935758.

Hassan, R., and Ho, M. (2008). Mesothelin targeted cancer immunotherapy. *Eur. J. Cancer* 44 (1), 46–53. Epub 2007 Oct 22. PMID: 17945478; PMCID: PMC2265108. doi:10.1016/j.ejca.2007.08.028

Hassan, R., Remaley, A. T., Sampson, M. L., Zhang, J., Cox, D. D., Pingpank, J., et al. (2006). Detection and quantitation of serum mesothelin, a tumor marker for patients with mesothelioma and ovarian cancer. *Clin. Cancer Res.* 12 (2), 447–453. PMID: 16428485. doi:10.1158/1078-0432.CCR-05-1477

Hassan, R., Schweizer, C., Lu, K. F., Schuler, B., Remaley, A. T., Weil, S. C., et al. (2010). Inhibition of mesothelin-CA-125 interaction in patients with mesothelioma by the anti-mesothelin monoclonal antibody MORAb-009: implications for cancer therapy. *Lung Cancer* 68 (3), 455–459. Epub 2009 Sep 9. PMID: 19744744; PMCID: PMC2864325. doi:10.1016/j.lungcan.2009.07.016

Hassan, R., Thomas, A., Alewine, C., Le, D. T., Jaffee, E. M., and Pastan, I. (2016). Mesothelin immunotherapy for cancer: ready for prime time? *J. Clin. Oncol.* 34 (34), 4171–4179. Epub 2016 Oct 31. PMID: 27863199; PMCID: PMC5477819. doi:10.1200/JCO.2016.68.3672

Heynickx, N., Segers, C., Coolkens, A., Baatout, S., and Vermeulen, K. (2023). Characterization of non-specific uptake and retention mechanisms of [177Lu]Lu-PSMA-617 in the salivary glands. *Pharmaceuticals* 16, 692. doi:10.3390/ph16050692

Ho, M., Feng, M., Fisher, R. J., Rader, C., and Pastan, I. (2011). A novel high-affinity human monoclonal antibody to mesothelin. *Int. J. Cancer* 128 (9), 2020–2030. PMID: 20635390; PMCID: PMC2978266. doi:10.1002/ijc.25557

Hollevoet, K., Reitsma, J. B., Creaney, J., Grigoriu, B. D., Robinson, B. W., Scherpereel, A., et al. (2012). Serum mesothelin for diagnosing malignant pleural mesothelioma: an individual patient data meta-analysis. *J. Clin. Oncol.* 30 (13), 1541–1549. Epub 2012 Mar 12. PMID: 22412141; PMCID: PMC3383122. doi:10.1200/JCO.2011.39.6671

Hucl, T., Brody, J. R., Gallmeier, E., Iacobuzio-Donahue, C. A., Farrance, I. K., and Kern, S. E. (2007). High cancer-specific expression of mesothelin (MSLN) is attributable to an upstream enhancer containing a transcription enhancer factor dependent MCAT motif. *Cancer Res.* 67 (19), 9055–9065. PMID: 17909009. doi:10.1158/0008-5472.CAN-07-0474

Kaneko, O., Gong, L., Zhang, J., Hansen, J. K., Hassan, R., Lee, B., et al. (2009). A binding domain on mesothelin for CA125/MUC16. *J. Biol. Chem.* 284 (6), 3739–3749. Epub 2008 Dec 15. PMID: 19075018; PMCID: PMC2635045. doi:10.1074/jbc.M806776200

Katsantoni, E. Z., Anghelescu, N. E., Rottier, R., Moerland, M., Antoniou, M., de Crom, R., et al. (2007). Ubiquitous expression of the rtTA2S-M2 inducible system in transgenic mice driven by the human hnRNPA2B1/CBX3 CpG island. *BMC Dev. Biol.* 7 (7), 108. PMID: 17900353; PMCID: PMC2080639. doi:10.1186/1471-213X-7-108

Lamberts, L. E., Menke-van der Houven van Oordt, C. W., ter Weele, E. J., Bensch, F., Smeenk, M. M., Voortman, J., et al. (2016). ImmunoPET with anti-mesothelin antibody in patients with pancreatic and ovarian cancer before anti-mesothelin antibody-drug conjugate treatment. *Clin. Cancer Res.* 22 (7), 1642–1652. Epub 2015 Nov 20. PMID: 26589435. doi:10.1158/1078-0432.CCR-15-1272

Lin, I., Rupert, P. B., Pilat, K., Ruff, R. O., Friend, D. J., Chan, M. K., et al. (2023). Novel mesothelin antibodies enable crystallography of the intact mesothelin ectodomain and engineering of potent, T cell-engaging bispecific therapeutics. *Front. Drug Discov.* 3, 2023. doi:10.3389/fddsv.2023.1216516

Liu, L., and Chen, J. (2022). Therapeutic antibodies for precise cancer immunotherapy: current and future perspectives. *Med. Rev.* 2 (6), 555–569. doi:10.1515/mr-2022-0033

Liu, X. F., Onda, M., Schlomer, J., Bassel, L., Kozlov, S., Tai, C. H., et al. (2024). Tumor resistance to anti-mesothelin CAR-T cells caused by binding to shed mesothelin is overcome by targeting a juxtamembrane epitope. *Proc. Natl. Acad. Sci. U. S. A.* 121, e2317283121. doi:10.1073/pnas.2317283121

Mahajan, S., Grewal, R. K., Friedman, K. P., Schöder, H., and Pandit-Taskar, N. (2022). Assessment of salivary gland function after 177Lu-PSMA radioligand therapy: current concepts in imaging and management. *Transl. Oncol.* 21, 101445. Epub 2022 May 3. PMID: 35523007; PMCID: PMC9079342. doi:10.1016/j.tranon.2022.101445

Nagy, A., Gertsenstein, M., Vintersten, K., and Behringer, R. (2003) "Manipulating the mouse embryo," in *A laboratory manual*. 3nd Edn. New York: Cold Spring Harbor Laboratory Press.

Pastan, I., and Hassan, R. (2014). Discovery of mesothelin and exploiting it as a target for immunotherapy. *Cancer Res.* 74 (11), 2907–2912. Epub 2014 May 13. PMID: 24824231; PMCID: PMC4062095. doi:10.1158/0008-5472.CAN-14-0337

Robinson, B. W., Creaney, J., Lake, R., Nowak, A., Musk, A. W., de Klerk, N., et al. (2003). Mesothelin-family proteins and diagnosis of mesothelioma. *Lancet* 362 (9396), 1612–1616. PMID: 14630441. doi:10.1016/S0140-6736(03)14794-0

Rottey, S., Clarke, J., Aung, K., Machiels, J. P., Markman, B., Heinhuis, K. M., et al. (2022). Phase I/IIa trial of BMS-986148, an anti-mesothelin antibody-drug conjugate, alone or in combination with nivolumab in patients with advanced solid tumors. *Clin. Cancer Res.* 28 (1), 95–105. Epub 2021 Oct 6. PMID: 34615718; PMCID: PMC9401510. doi:10.1158/1078-0432.CCR-21-1181

Roy, J., Warner, B. M., Basuli, F., Zhang, X., Zheng, C., Goldsmith, C., et al. (2021). Competitive blocking of salivary gland [^{18}F]DCFPyL uptake via localized, retrograde ductal injection of non-radioactive DCFPyL: a preclinical study. *EJNMMI Res.* 11 (1), 66. PMID: 34287731; PMCID: PMC8295433. doi:10.1186/s13550-021-00803-9

Scholler, N., Fu, N., Yang, Y., Ye, Z., Goodman, G. E., Hellström, K. E., et al. (1999). Soluble member(s) of the mesothelin/megakaryocyte potentiating factor family are detectable in sera from patients with ovarian carcinoma. *Proc. Natl. Acad. Sci. U. S. A.* 96 (20), 11531–11536. PMID: 10500211; PMCID: PMC18068. doi:10.1073/pnas.96.20.11531

Sun, Z., Chu, X., Adams, C., Ilina, T. V., Guerrero, M., Lin, G., et al. (2023). Preclinical assessment of a novel human antibody VH domain targeting mesothelin as an antibody-drug conjugate. *Mol. Ther. - Oncolytics* 31, 100726. doi:10.1016/j.omto.2023.09.002

Tang, Z., Feng, M., Gao, W., Phung, Y., Chen, W., Chaudhary, A., et al. (2013). A human single-domain antibody elicits potent antitumor activity by targeting an epitope in mesothelin close to the cancer cell surface. *Mol. Cancer Ther.* 12 (4), 416–426. Epub 2013 Jan 31. PMID: 23371858; PMCID: PMC3624043. doi:10.1158/1535-7163.MCT-12-0731

Ter Weele, E. J., van Scheltinga, A. G. T., Kosterink, J. G. W., Pot, L., Vedelaar, S. R., Lamberts, L. E., et al. (2015). Imaging the distribution of an antibody-drug conjugate constituent targeting mesothelin with 89Zr and IRDye 800CW in mice bearing human pancreatic tumor xenografts. *Oncotarget* 6 (39), 42081–42090. PMID: 26536664; PMCID: PMC4747211. doi:10.18632/oncotarget.5877

Vidarsson, G., Dekkers, G., and Rispens, T. (2014). IgG subclasses and allotypes: from structure to effector functions. *Front. Immunol.* 5, 520. ISSN=1664-3224. doi:10.3389/fimmu.2014.00520

Yakushiji, H., Kobayashi, K., Takenaka, F., Kishi, Y., Shinohara, M., Akehi, M., et al. (2019). Novel single-chain variant of antibody against mesothelin established by phage library. *Cancer Sci.* 110 (9), 2722–2733. Epub 2019 Aug 28. PMID: 31461572; PMCID: PMC6726835. doi:10.1111/cas.14150

Zhan, J., Lin, D., Watson, N., Esser, L., Tang, W. K., Zhang, A., et al. (2023). Structures of cancer antigen mesothelin and its complexes with therapeutic antibodies. *Cancer Res. Commun.* 3 (2), 175–191. PMID: 36968141; PMCID: PMC10035497. doi:10.1158/2767-9764.CRC-22-0306

Zhang, J., Bera, T. K., Liu, W., Du, X., Alewine, C., Hassan, R., et al. (2014). Megakaryocytic potentiating factor and mature mesothelin stimulate the growth of a lung cancer cell line in the peritoneal cavity of mice. *PLoS One* 9 (8), e104388. PMID: 25118887; PMCID: PMC4132110. doi:10.1371/journal.pone.0104388

Zhang, Y. F., Phung, Y., Gao, W., Kawa, S., Hassan, R., Pastan, I., et al. (2015). New high affinity monoclonal antibodies recognize non-overlappingepitopes on mesothelin for monitoring and treating mesothelioma. *Sci. Rep.* 5, 9928–10014. doi:10.1038/srep09928

Zhou, Q., Stefano, J. E., Manning, C., Kyazike, J., Chen, B., Gianolio, D. A., et al. (2014). Site-specific antibody-drug conjugation through glycoengineering. *Bioconjugate Chem.* 25 (3), 510–520. Epub 2014 Feb 28. PMID: 24533768. doi:10.1021/bc400505q